Design of Soft-X Ray Imaging System for Magnetic Islands of RFP Plasmas

Akio SANPEI, Takumi ONCHI, Ryuya IKEZOE,
Haruhiko HIMURA and Sadao MASAMUNE

Department of Electronics, Kyoto Institute of Technology, Kyoto 606-8585, Japan

(Received 10 December 2006 / Accepted 23 May 2007)

A soft X ray (SXR) imaging system for diagnosing magnetic islands of a reversed field pinch (RFP) plasma is proposed. The SXR imaging system utilizes a microchannel plate (MCP) to record a higher-resolution distribution of two-dimensional (2D) luminosity on a phosphor plate. In order to identify the structure of the magnetic island from the obtained SXR image, we have calculated the 2D image expected from RFP plasmas. It is found that the 2D image reflects the change in the radiation intensity caused by the magnetic island. Also, the magnetic island can be distinguished clearly when the radiation power emitted from the magnetic island is more than about 20 % of that on the magnetic axis of RFP. Regarding with the view angle α of the SXR imaging system, the magnetic island due to a tearing mode on the $m = 1/n = 8$ rational surface can be detected as far as $\alpha > \pi/10$.

Keywords: RFP, soft-x ray, imaging, magnetic island

DOI: 10.1585/pfr.2.S1064

1. Introduction

The measurement of bremsstrahlung soft-x ray (SXR) radiation is one of useful passive methods for diagnosing high-temperature plasmas [1–3], because contours of the SXR emissivity correspond to magnetic surfaces of the plasmas. In addition, the SXR computer tomography (SXR-CT) technique [4] has been used widely, and with it, the magnetic structures of the plasmas are successfully reconstructed [5]. For reversed field pinch (RFP) plasmas, on the other hand, a method using a surface barrier diode (SBD) array [6] has been applied to measure the SXR distribution of the plasmas. However, one of disadvantages of this method is that a large number of SXR detectors is required in order to obtain the three-dimensional (3D) structure of magnetic islands of RFP, and moreover, the spatial resolution is limited in a narrow region.

Since the safety factor of RFP is less than unity, the toroidal pitch of the magnetic field lines results in relatively short, and instabilities with high n and low m mode numbers appear in the plasmas. These imply that an SXR imaging system with a microchannel plate (MCP), which provides a higher resolution of the SXR distribution, would be adequately applied to the RFP for answering the dynamical structure of magnetic islands of RFP.

In this study, we propose a new SXR imaging system with an MCP for taking two-dimensional (2D) SXR images of RFP. The SXR imaging system utilizes a pinhole camera to record higher-resolution distribution of the luminosity on a phosphor plate. The obtained 2D image is amplified with a high-speed image intensifier charged coupled device (ICCD). Moreover, assuming both SXR emission profiles and a magnetic island on a rational surface of RFP, we have calculated the 2D SXR image expected from them. On the basis of the calculation, a proto-type 2D SXR imaging system for STE-2 [7–9] RFP plasma has been developed [10].

The outline of this paper is as follows. In Sec. 2, we describe the design of the proposed SXR imaging system. Quantitative analyses are explained in terms of both the threshold of minimum sensitivity for measuring the radiation power emitted from magnetic islands of RFP and the view angle of the system in Sec. 3. Finally, a summary is given in Sec. 4.

2. Design of SXR Imaging System with MCP

The SXR imaging system designed here consists of four parts: a pinhole, the MCP (Hamamatsu Photonics F2222-21P), a phosphor plate and an ICCD camera. A Schematic drawing of the SXR imaging system is illustrated in Fig. 1. The pinhole is placed at 35 mm horizontally (along the major radius) away from the plasma edge. And, the diameter of the it is 1.0 mm. Before passing through the pinhole, SXR is filtered by polyester foils which provide the energy spectrum of SXR. The SXR image is then created on the surface of the MCP separated from the pinhole by 50 mm.

A 2D distribution of photoelectrons induced by the SXR at photocathodes of the MCP is amplified in dynodes with 20 mm diameters. And, the anode electron is accelerated again by electrostatic potential with 2.0 kV, before

author's e-mail: sanpei@kit.ac.jp

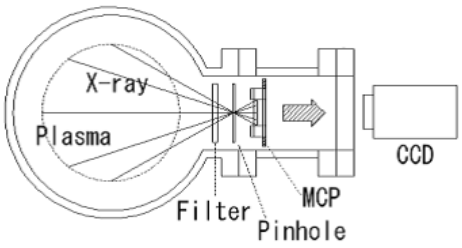

Fig. 1 A schematic illustration of the 2D SXR imaging system. It utilizes a pinhole, an MCP, a phosphor plate and an ICCD camera. The filter is made of polyester.

hitting the phosphor screen where a visible light image of the secondary electron distribution appears. In this system, the conversion efficiency of MCP is 15 % and the practical gain is 2.0×10^4. The 2D luminosity distribution on the phosphor plate is taken with the high-speed ICCD camera with a 385×579 pixels array and recorded in a computer as 32 bits of the dynamic range. Nevertheless, the SXR image is produced only in a limited area on the array: 150×150 pixels. The sensitivity of the ICCD camera can be controlled by changing the exposure time t_{ex}. In most cases, we set t_{ex} to be 5 μs.

Since magnetic islands are evolved on rational surfaces, the strength of the SXR radiation strongly dependson them [11]. Figure 2 (a) and (b) indicate typical magnetic surfaces and magnetic islands at a poloidal cross section of RFP, and the 3D plot of the magnetic islands, respectively. The magnetic island width w due to the corresponding m/n tearing mode can be estimated as

$$W = 4r_{mn}\left[\frac{B_r^1}{mB_\theta}\left(\frac{q}{rq'}\right)\Big|_{r_{mn}}\right]^{1/2}, \qquad (1)$$

where B_r^1 is the fluctuation component of B_r for the corresponding tearing mode. When the w of neighboring islands are sufficiently broad, they are overlapped each other, resulting in a stochastic magnetic field. In this case, magnetic islands may not be observed with the proposed imaging system. On the other hand, when the overlapping doesn't occur, a 2D image reflecting internal magnetic islands is expected to be obtained.

3. Calculation of 2D Image

In order to identify magnetic islands of RFP with referring the SXR image, we have at first estimated the 2D image expected from RFP plasmas. In calculations, profiles of the radiation power from both the bulk plasma P_{rad-bg} and the magnetic island P_{rad-mi} are assumed as follows. Considering a cylindrical plasma, values of the electron density $n_e(0)$, the electron temperature $T_e(0)$, and $P_{rad-bg}(0)$ on the plasma axis are assumed to be $1.00 \times 10^{19}/\mathrm{m}^3$, 1.00×10^2 eV, and 5.72×10^{-17} W/cm^3, respectively. Only one magnetic island due to a tearing mode on the $m = 1/n = 8$ rational surface at $r/a = 0.4$ is assumed,

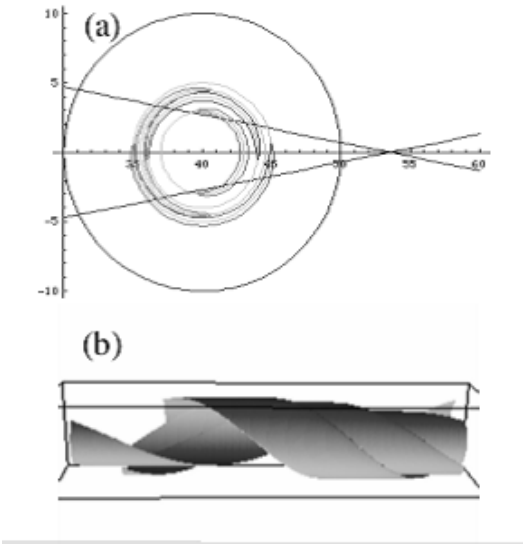

Fig. 2 (a): Schematic drawings of magnetic islands in a poloidal cross section of a cylindrical plasma. The solid lines correspond to the lines of sights. (b): A 3D plot of magnetic islands due to tearing modes.

where a is minor radius. The power of the bremsstrahlung SXR radiation P_{rad} is written as [1]

$$P_{rad} = 1.54 \times 10^{-32} n_e n_i Z^2 (\kappa T_e)^{1/2} \overline{g_{ff}}(Z, T_e), \qquad (2)$$

where n_i is the ion density, Z is the effective ion charge and $\overline{g_{ff}}$ is the temperature averaged free-free Gaunt factor. Here, n_e and n_i are assumed to be equal and Z is unity. Therefore, $P_{rad}(x, y)$ can be decided from $n(x, y)$ and $T_e(x, y)$. Also, as seen from eq. (2), P_{rad} is proportional to n_e^2 and $T_e^{1/2}$.

Regarding with the procedure of calculating the 2D image, $P_{rad}(x, y)$ is, at first, numerically distributed to the voxel array, that is, $64 \times 64 \times 64$ voxels. Secondly, we calculate $I_i = \int \vec{P_{rad}} \cdot \vec{dl} (= V_i \times L_i)$ of the ith voxel. Here, V_i is the initial value of $P_{rad}(x, y)$ in the ith voxel and L_i is the length of path of SXR there. Thirdly, I_i is divided by l^2 where l is the distance between the voxel and MCP. After calibrating inherent sensibility of MCP for incident angle of SXR, the value of I_i/l^2 is summed over along the line of sight. Finally, the 2D image of SXR distribution $P_{img}(x, y)$ is obtained.

Typical 2D images calculated are shown in Figs. 3, 4 and 5, which show the dependences of $P_{img}(x, y)$ on the values $P_{rad-mi}(0)$, the 3D structure of the magnetic island, and view angle α of the SXR imaging system, respectively. To emphasize the contrast of each image, the color-coding of it is adjusted appropriately. Figure 3(a) shows a typical $P_{img}(x, y)$ without the magnetic island when $P_{rad-bg}(x, y)$ is a Gaussian. On the other hand, when the magnetic island due to the tearing mode is included, the calculated 2D image reflects the existence of the magnetic island. is considerably changed. Figure 3(b) and (c) show the re-

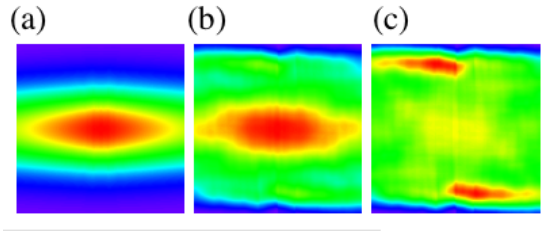

Fig. 3 2D intensity distributions of the radiation power emitted from the cylindrical plasma (a) without any magnetic island, (b) with a magnetic island having the radiation power of 5.00×10^{-17} W/cm^3, and (c) with a magnetic island having the radiation power of 1.00×10^{-16} W/cm^3.

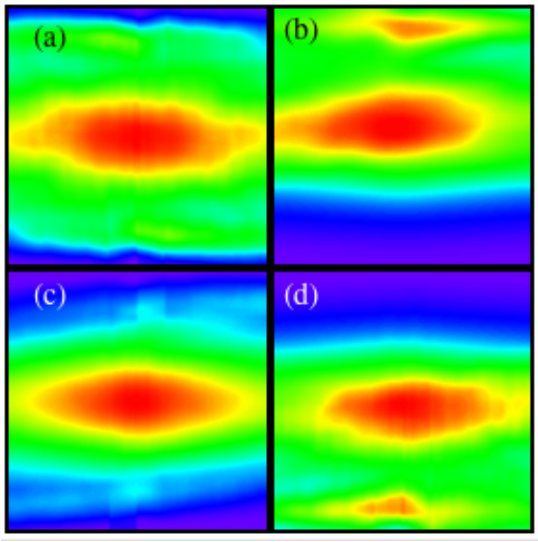

Fig. 4 2D intensity distributions for θ = (a) 0, (b) $\pi/2$, (c) π, and (d) $3\pi/2$.

sults when $P_{rad-mi}(0)$ is (b) 5.00×10^{-17} W/cm^3 and (c) 1.00×10^{-16} W/cm^3, respectively. Comparing with them, it is recognized that the peak of intensity moves to the vertical direction as P_{rad-mi} increases.

To evaluate a threshold of P_{rad-mi} with regard to the 3D structure of the magnetic island, several calculations of 2D images are performed by changing azimuthal angle θ of the magnetic island. Here, when the magnetic island reaches its closest point to the pinhole, the value of θ is defined to be 0. Values of $P_{rad-bg}(0)$ and $P_{rad-mi}(0)$ are the same as those used for the calculation of Fig. 3(b). As recognized from Fig. 4, the magnetic island clearly appears, when θ is $\pi/2$ or $3\pi/2$. On the other hand, for cases where $\theta = 0, \pi$, P_{rad-mi} seems to overlap P_{rad-bg}, which suggests that the magnetic island is hard to be observed. In fact, a preliminary calculation including uncertain of P_{rad-bg} has revealed that P_{rad-mi} should be more than about 20 % of $P_{rad-bg}(0)$.

Next, the dependence of the calculated SXR image on α is examined. Though α is required to be $\pi/4$ to observe a whole structure of the $m = 1/n = 8$ mode, such a

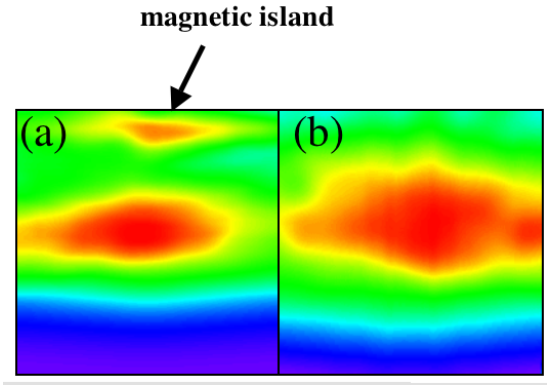

Fig. 5 2D intensity distributions for α = (a) $\pi/10$, (b) $\pi/20$.

large value is not needed to see whether the magnetic island exists or not. Figure 5(a) and (b) show $P_{img}(x, y)$ for cases where α is (a) $\pi/10$, and (b) $\pi/20$, respectively. For $\alpha = \pi/10$, the magnetic island is clearly observed at the top of Fig. 5 (a). However, when α is too small, the magnetic island can not be seen. As recognized from Fig. 5 (b), peak of intensity due to P_{rad-mi} moves outwardly.

4. Summary

In order to observe a magnetic island on a rational surface of an RFP plasma, we have proposed a new SXR imaging system. It utilizes an MCP with ICCD to record higher-resolution distribution of 2D luminosity on a phosphor plate. In order to identify the magnetic island with referring the SXR image, we estimate the 2D image expected from RFP plasmas. From the calculation, it is revealed that the magnetic island can be distinguished clearly when the radiation power emitted from the magnetic island is more than about 20 % of that on the magnetic axis of RFP. Regarding with the view angle α of the SXR imaging system, the magnetic island due to a tearing mode on the $m = 1/n = 8$ rational surface can be detected as far as $\alpha > \pi/10$.

Acknowledgments

This work is supported by a grant for young researchers of Kyoto Institute of Technology, and is partly supported by the Sasakawa Scientific Research Grant from The Japan Science Society.

[1] I.H. Hutchinson, *Principles of Plasma Diagnostics* Cambridge University Press, Cambridge (1987).
[2] T. Nash, C. Deeney, P.D. LePell, R. Prasad and M. Krishnan, Rev. Sci. Instrum. **61**, 2807 (1990).
[3] E.A. Crowford, D.P. Taggart and A.D. Bailey III, Rev. Sci. Instrum. **61**, 2795 (1990).
[4] N.R. Sauthoff, S. von Goeler and W.F. Stodiek, Nucl. Fusion **18**, 1445 (1985).
[5] R.Z. Granetz and J.F. Camacho, Nucl. Fusion **25**, 727 (1985).
[6] H. Koguchi *et al.*, Rev. Sci. Instrum. **75**, 4004 (2004).

[7] S. Masamune, M. Iida, N. Oda, K. Fujitsuka, M. Awazu, K. Ohta, H. Oshiyama, Fusion Energy **21**, 201 (1996).
[8] S. Masamune, M. Iida, Y. Ohfuji, K. Ohta, H. Oshiyama, Plasma Phys. Control. Fusion **40**, 127 (1998).
[9] S. Masamune and M. Iida, J. Plasma Fusion Res. SERIES **5**, 509 (2002).
[10] T. Onchi, A. Sanpei, R. Ikezoe *et al.*, *poster P6-26 in this conference*.
[11] P. Franz, L. Marrelli, P. Piovesan *et al.*, Phys. Rev. Lett. **92**, 125001 (2004).